

Thionin as a Bipolar Organic Cathode Material for Aqueous Rechargeable Zinc Batteries

Pu Yu,^[a] Junxiao Wang,^[a] Xiaotang Gan,^[a] Zhihua Guo,^[a] Liang Huang,^[a] and Zhiping Song^{*[a]}

Organic cathode materials (OCMs) have been widely applied in aqueous rechargeable zinc batteries (ARZBs), but there are still many novel structures to be explored for better electrochemical performance and clearer mechanism. Herein, we have studied an organic biological dye, namely thionin (Thn-CH₃COO), as a bipolar-type OCM for ARZBs based on its electroactive phenothiazine unit. In the optimal electrolyte of 2 M Zn-(CF₃SO₃)₂, Thn-CH₃COO exhibited the lowest solubility and thus the highest cycling stability (94% capacity retention after 100

cycles), with a reversible capacity of 162 mAh g⁻¹ (the theoretical value is 186 mAh g⁻¹) and a discharge plateau at ~0.8 V vs. Zn²⁺/Zn. Various characterization and DFT calculations have revealed that both CH₃COO⁻ and CF₃SO₃⁻ anions and H⁺ cations participated the p-type and n-type reactions, respectively. In brief, the novel structure, competitive performance, and exhaustive mechanism investigation will facilitate the further development of ARZBs based on OCMs.

Introduction

Aqueous rechargeable zinc batteries (ARZBs) based on Zn metal anode (820 mAh g⁻¹) and aqueous electrolyte are regarded as one of the most promising battery technologies for large-scale energy storage due to their intrinsic safety and potentially low cost.^[1] In the past decade, various cathode materials have been investigated for ARZBs, including inorganics and organics. Compared with inorganic cathode materials (OCMs) mainly based on Mn and V, organic cathode materials (OCMs) possess many advantages including higher structure diversity and designability, higher structure stability in aqueous electrolyte, and higher resource sustainability.^[2] Moreover, it has been found that many small-molecule organic cathode materials (SMOCMs) exhibited much lower solubility and much higher cycling stability in ARZBs with weakly acidic electrolytes than in rechargeable lithium and sodium batteries with non-aqueous electrolytes. Therefore, the combination of ARZBs and OCMs provide both of them huge opportunities towards higher electrochemical performance for practical application.^[3]

Generally, according to the electrochemical redox mechanisms, OCMs can be classified into three types: n-type, p-type, and bipolar-type.^[4] n-Type molecules in neutral state are firstly reduced to anions in discharge process, which combine with cations from the electrolyte to achieve charge neutralization. Depending on structure of the active material and nature of the electrolyte, the embedded cations are possibly Zn²⁺, H⁺,

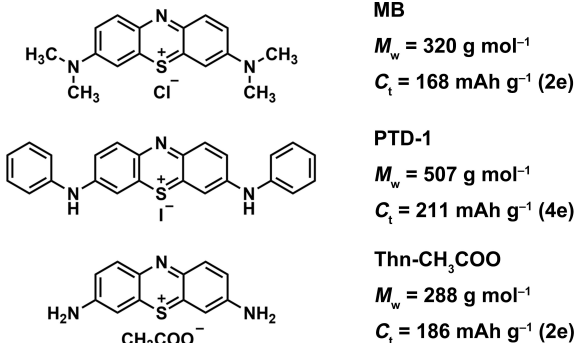
Zn(CF₃SO₃)⁺ ions, etc.^[5] On the contrast, p-type molecules in neutral state are firstly oxidized to cations in charge process and associate with anions from the electrolyte, including SO₄²⁻, CF₃SO₃⁻, CH₃COO⁻, etc. Bipolar-type molecules are those possess both n-type and p-type characters and thus can be either discharged or charged firstly, with the participation of both cations and anions. Among the three types, n-type OCMs have been paid the most attentions because of their abundant structures (mainly based on carbonyl and imine, e.g., TAPQ,^[6] TABQ,^[7] PQ-Δ,^[8] and DTT^[9]) and high capacities. However, a lot of works have proved that the dominantly embedded cation for OCMs is actually H⁺ rather than the expected Zn²⁺, which is also the case for many inorganic cathode materials.^[10] The consumption of H⁺ from the electrolyte leads to the precipitation of basic zinc salt like Zn₄SO₄(OH)₆·5H₂O^[11] and Zn_x-(CF₃SO₃)_{2x-y}(OH)_y·nH₂O.^[12] Although this behavior is reversible in the charge process, it significantly reduces the actual specific capacity and energy at the cell level because that the considerable molecular weight of the by-product [92 g mol⁻¹ per electron for Zn₄SO₄(OH)₆·5H₂O, and probably higher value for Zn_x(CF₃SO₃)_{2x-y}(OH)_y·nH₂O] should be taken into account in the calculation. In this respect, although p-type and bipolar-type OCMs involve anions with remarkable molecular weight (e.g., 48 and 149 g mol⁻¹ for 1/2 SO₄²⁻ and CF₃SO₃⁻, respectively), their actual capacities and energy densities may be comparable to those of n-type ones.

In fact, many OCMs that are recognized as p-type ones for non-aqueous batteries, e.g., polyaniline (PAni)^[13] and poly(diaminonaphthalene)^[14] with conjugated amine groups, possess bipolar behaviors in ARZBs. Another type of bipolar electroactive unit is phenothiazine, and the reported examples include methylene blue (MB)^[15] and PTD-1^[16] (Scheme 1). Besides them, there is another phenothiazine-based molecule, namely thionin (Thn-CH₃COO; Scheme 1), has not been explored as OCMs for rechargeable batteries yet. Like MB, it is also a commercially available biological dye (also known as Lauth's violet), but has a higher theoretical capacity than MB

[a] P. Yu, J. Wang, X. Gan, Z. Guo, L. Huang, Prof. Z. Song
Hubei Key Lab of Electrochemical Power Sources
College of Chemistry and Molecular Sciences
Wuhan University
Wuhan 430072 (China)
E-mail: zpsong@whu.edu.cn
Homepage: <http://zpsong.whu.edu.cn/english.html>

Supporting information for this article is available on the WWW under
<https://doi.org/10.1002/batt.202300010>

An invited contribution to a Special Collection on Organic Batteries.



Scheme 1. Molecular structures, molecular weights, and theoretical specific capacities of the three phenoxythiazine-based bipolar organic electrode materials (MB, PTD-1, and Thn-CH₃COO).

(186/235 mAh g⁻¹ vs. 168/188 mAh g⁻¹ for the moiety with/without anion). Therefore, herein we have systematically investigated this material as a novel organic cathode for ARZBs. The electrolyte composition has been optimized to improve the cycling stability, and the redox reaction and electrode evolution mechanisms have been studied in depth via various electrochemical and *ex-situ* characterization methods. We believe this work provides new understandings of phenoxythia-

zine-based and bipolar OCMs for ARZBs, which are important for their further development.

Results and Discussion

Actually, there are mainly two different structures of thionin, with Cl⁻ and CH₃COO⁻ as the associated anion, respectively. However, only the one with CH₃COO⁻ is commercially available. In order to distinguish this and the related molecules in the later discussion, the pristine thionin was named as Thn-CH₃COO. Compared with its analogues based on phenothiazine unit (Scheme 1), it has many advantages in theory. Firstly, replacing the $-\text{N}(\text{CH}_3)_2$ groups of MB by $-\text{NH}_2$ not only reduces the molecular weight and thus increases the theoretical capacity, but may also enhance the structure stability during discharge-charge process through the intermolecular hydrogen bonds. Secondly, although CH₃COO⁻ has a higher molecular weight than Cl⁻, it is more stable at high potential (under which Cl⁻ will be oxidized),^[17] and an electrolyte with the same anion [Zn(CH₃COO)₂] can be used for it to eliminate the possible anion exchange (ZnCl₂ is also applicable, but the anion is mainly ZnCl₃⁻ rather than Cl⁻).^[18] Thirdly, although Thn-CH₃COO has a smaller theoretical capacity than PTD-1, it does not need complicated synthesis as for PTD-1, and the structure

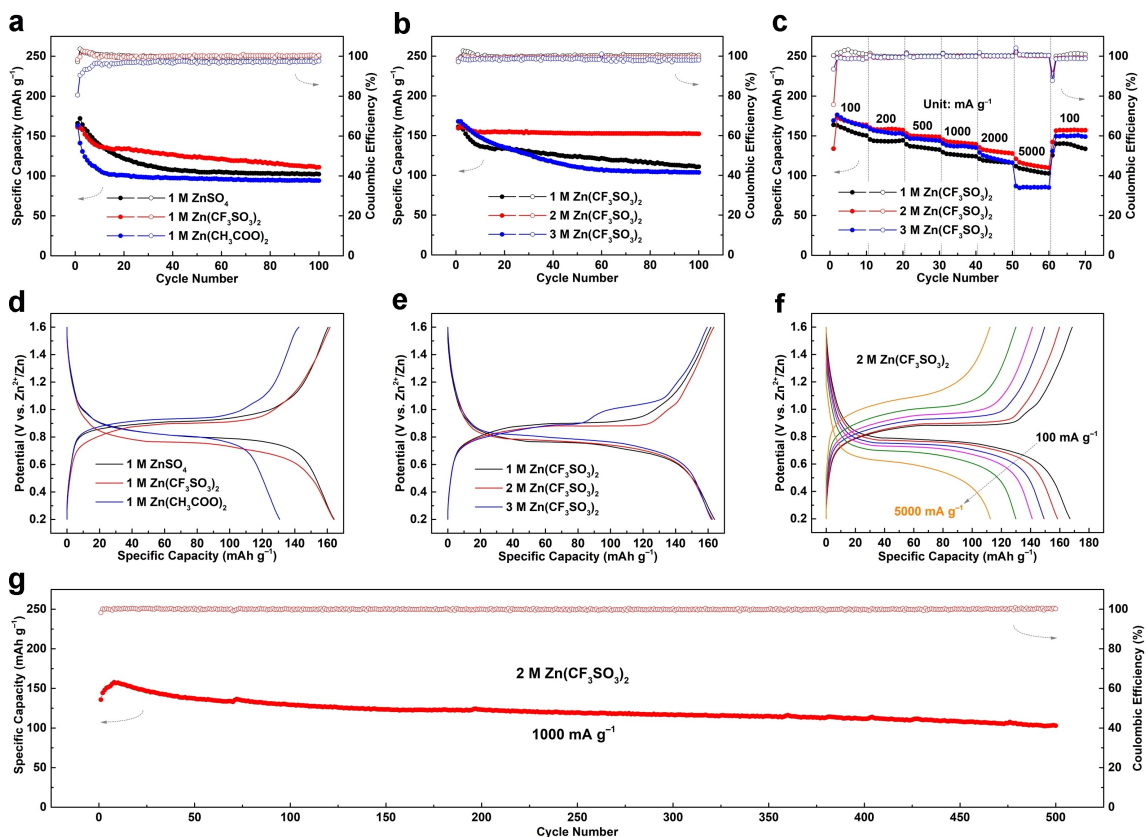


Figure 1. Galvanostatic discharge-charge performance of Thn-CH₃COO: a, b) cycling performance under a current rate of 100 mA g⁻¹, in different electrolytes of a) 1 M ZnSO₄/Zn(CF₃SO₃)₂/Zn(CH₃COO)₂ and b) 1/2/3 M Zn(CF₃SO₃)₂, and d, e) the corresponding typical discharge-charge curves (of the 3rd cycle). c) Rate performance in different electrolytes of 1/2/3 M Zn(CF₃SO₃)₂ and f) the corresponding typical discharge-charge curves (of the 5th cycle at each current rate) in 2 M Zn(CF₃SO₃)₂ electrolyte under different current rates. g) Long-term cycling performance in 2 M Zn(CF₃SO₃)₂ electrolyte under 1000 mA g⁻¹.

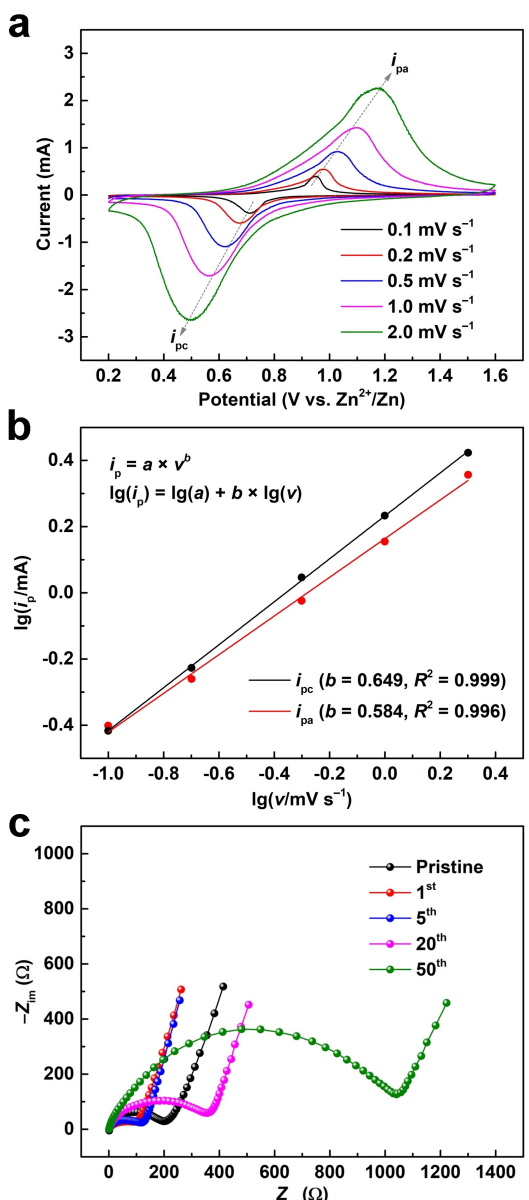


Figure 2. Electrochemical analysis of the Thn-CH₃COO electrode: a) typical CV curves at different scan rates, and b) the corresponding relations between $\lg(i_p)$ and $\lg(v)$, where i_p and v refer to the peak current and scan rate, respectively; c) EIS data (Nyquist plots) at charged state during cycling (under 100 mA g⁻¹).

is simpler for understanding the electrochemical behaviors of phenothiazine unit.

To investigate the electrochemical performance of Thn-CH₃COO as a cathode for ARZBs, we employed a cathode composition of Thn-CH₃COO/KB/PTFE = 6:3:1 (KB = Ketjenblack, PTFE = polytetrafluoroethylene), and different aqueous electrolytes including the commonly used zinc sulfate (ZnSO₄) and zinc trifluoromethanesulfonate [Zn(CF₃SO₃)₂], as well as the above mentioned zinc acetate [Zn(CH₃COO)₂]. The discharge-charge voltage window was set as 0.2–1.6 V to fully demonstrate the electroactivity of Thn-CH₃COO, and the current rate was set as 100 mA g⁻¹ unless otherwise specified. Firstly, we compared its cycling performance in different electrolytes with

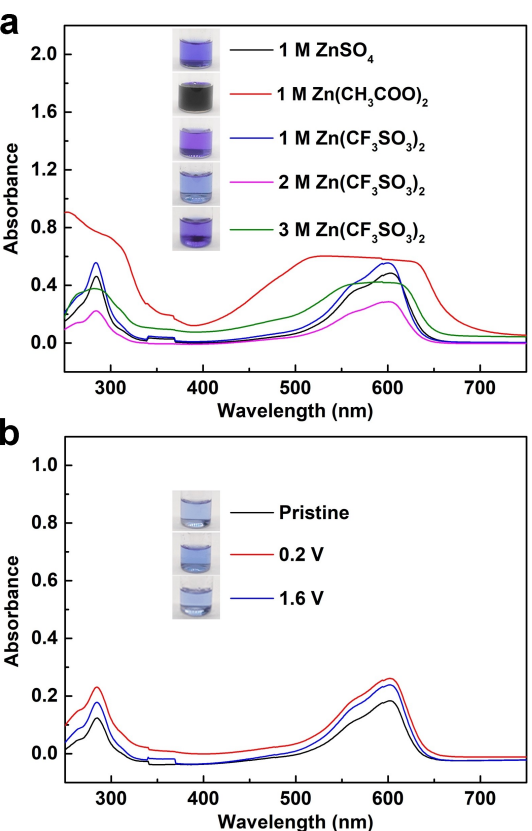


Figure 3. UV-Vis spectra of a) different electrolytes after immersing the pristine Thn-CH₃COO electrode for 24 h and b) the 2 M Zn(CF₃SO₃)₂ electrolytes after immersing the Thn-CH₃COO electrodes in different states (pristine, discharged to 0.2 V, and recharged to 1.6 V) for 24 h, with inserted photographs showing the dissolution phenomena.

the same concentration of 1 M (Figure 1a). In the three electrolytes, the reversible capacities (maximum discharge capacities) were almost the same (160–170 mA h g⁻¹), but the capacity retentions were 59%, 69%, and 58% in the ZnSO₄, Zn(CF₃SO₃)₂, and Zn(CH₃COO)₂ electrolytes, respectively. It was also found that the Coulombic efficiencies were much lower in the Zn(CH₃COO)₂ electrolyte, suggesting that the dissolution and shuttle effect of Thn-CH₃COO was more severe in it, although they have the same anion to avoid anion exchange. As for the corresponding discharge–charge curves (Figure 1d), a single voltage plateau at approximately 0.8 V (which is consistent with that of MB)^[15] was observed for all the electrolytes, but the one in the Zn(CF₃SO₃)₂ electrolyte was about 0.05 V lower than those in the other two electrolytes. It suggested that the thionin cation (Thn⁺) probably had weaker electrostatic interaction with CF₃SO₃⁻ than with SO₄²⁻ and CH₃COO⁻, which may be the origin of the higher cycling performance.^[19]

To further improve the cycling stability of Thn-CH₃COO, we adopted a “concentrated electrolyte” strategy for the optimized salt of Zn(CF₃SO₃)₂, considering that higher concentration is usually effective to suppress the dissolution of organic active materials.^[20] Figure 1(b) shows the cycling performance in the Zn(CF₃SO₃)₂ electrolytes with different concentrations of 1, 2, and 3 M. Obviously, the 2 M electrolyte led to the highest

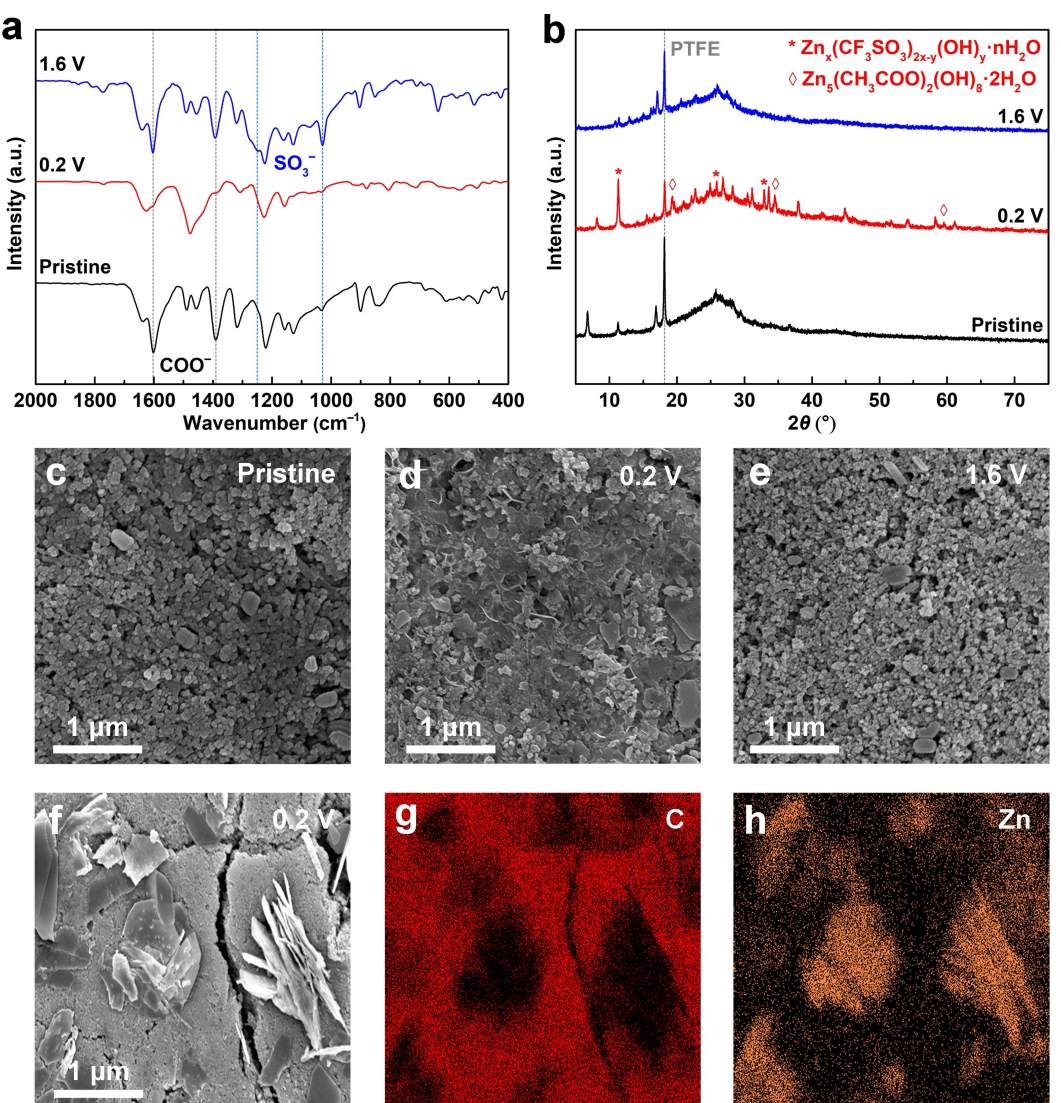


Figure 4. Ex-situ characterization results of the Thn-CH₃COO electrodes at different states (pristine, discharged to 0.2 V, and recharged to 1.6 V): a) FTIR spectra; b) XRD patterns; c–e) SEM images; f–h) SEM-EDS images of the electrode at 0.2 V.

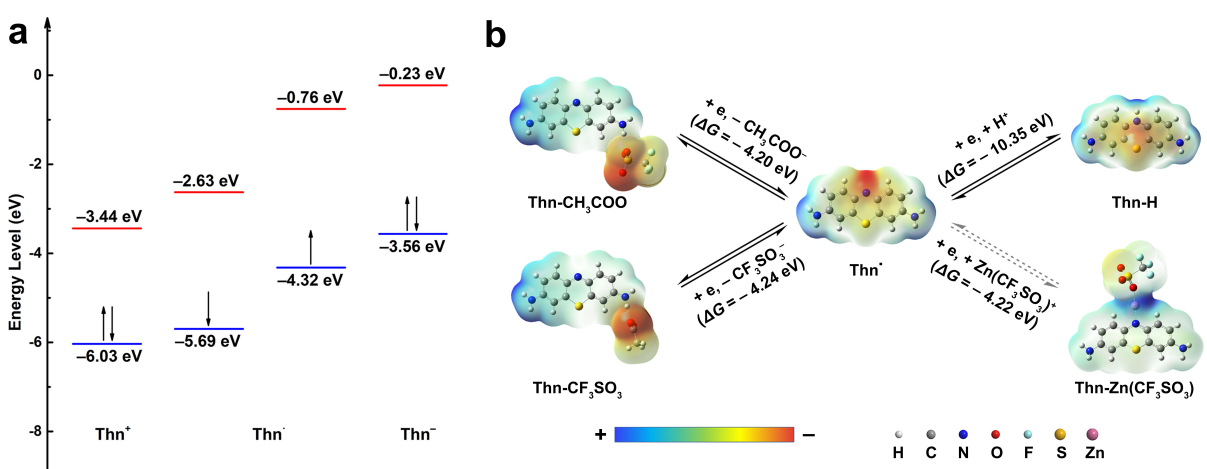


Figure 5. DFT calculation results of the thionin-related molecules: a) HOMO–LUMO energy levels of the naked molecules (Thn⁺, Thn⁰, and Thn⁻); b) proposed redox reaction mechanisms of Thn-CH₃COO, and the related geometrical configurations, MESP maps, and Gibbs free energy changes (ΔG).

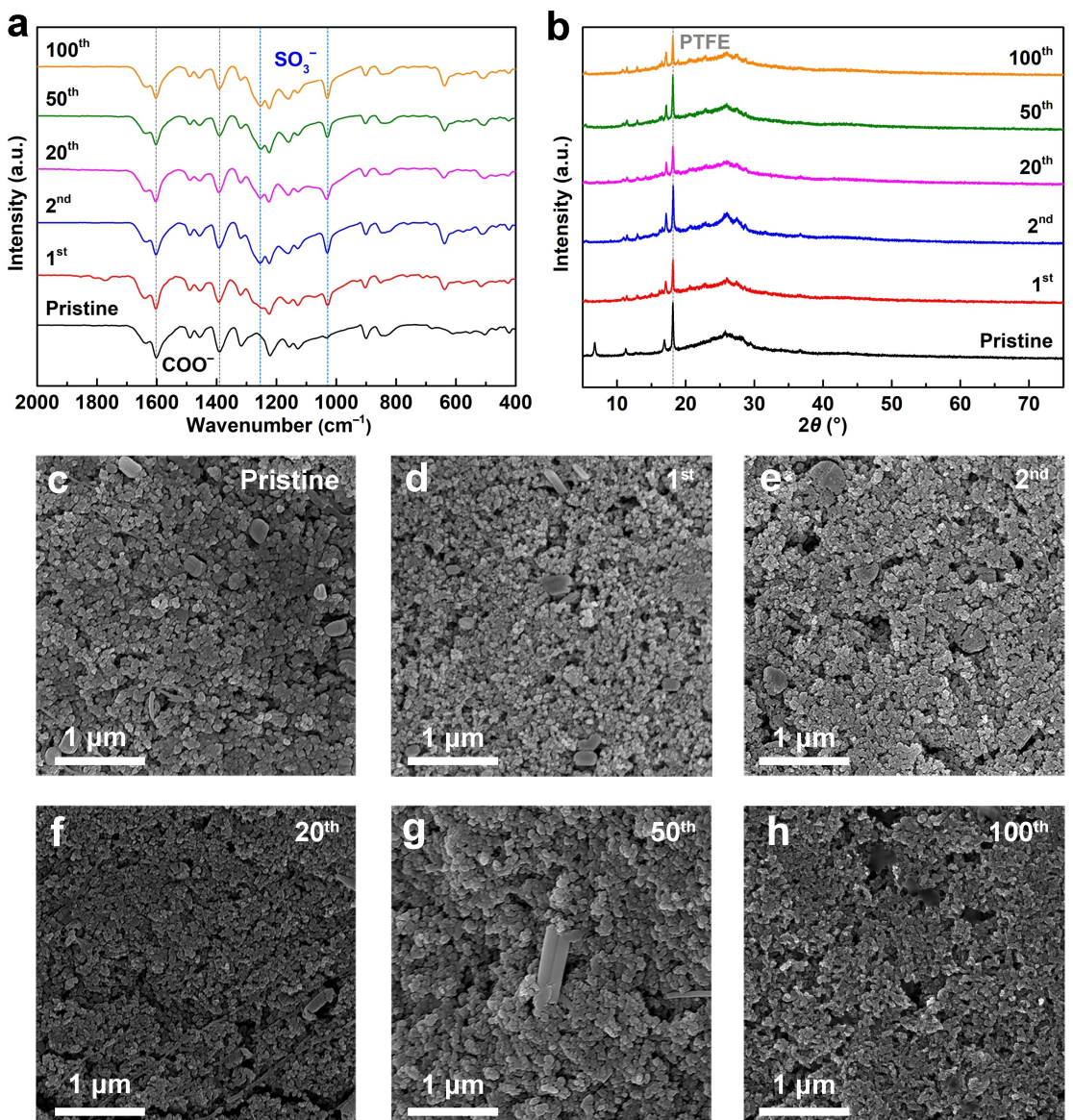


Figure 6. *Ex-situ* characterization results of the Thn-CH₃COO electrodes in charged state at different cycle numbers (pristine, 1, 2, 20, 50, and 100) to reveal the electrode structure evolution: a) FTIR spectra; b) XRD patterns; c-h) SEM images.

capacity retention of 94% after 100 cycles. It was unexpected that the 3 M electrolyte caused even faster capacity fading and lower Coulombic efficiencies. The corresponding discharge-charge curves (Figure 1e) showed that there was no remarkable voltage polarization after increasing the electrolyte concentration, except for the obviously elevated plateau at the second half of the charge process in the 3 M electrolyte (probably due to the inferior redeposited morphology of the active material in the highly concentrated electrolyte, which resulted in poorer electronic and/or ionic conduction). In the optimized electrolyte of 2 M Zn(CF₃SO₃)₂, the reversible capacity of Thn-CH₃COO was 162 mAh g⁻¹, which was higher than those of its analogues of MB and PTD-1 (Table S1). More precisely, after subtracting the capacity contribution of 15 mAh g⁻¹ from KB (Figure S1), the capacity utilization of Thn-CH₃COO was 79% (relative to the theoretical capacity of 186 mAh g⁻¹). It indicated that the two-

electron reaction of phenothiazine was almost completely utilized but some capacity was lost due to the dissolution of active material. The average discharge voltage was 0.74 V, which is at a moderate level of OCMs for ARZBs.

In addition, we compared the rate performance of Thn-CH₃COO in the Zn(CF₃SO₃)₂ electrolytes with different concentrations (Figure 1c). It was observed that the 2 M electrolytes also led to superior capacity retentions at higher current rates. The reason was, on one hand the faster capacity fading in the 1 M and 3 M electrolytes during cycling reduced the capacity retentions, on the other hand the higher viscosity of the 3 M electrolyte was adverse to the reaction kinetics.^[21] In the optimal 2 M electrolyte, the capacity retentions were 91%, 86%, 82%, 75%, and 70% relative to the capacity at 100 mA g⁻¹ under increasing current rates of 200, 500, 1000, 2000, and 5000 mA g⁻¹, respectively. The corresponding dis-

charge–charge curves (Figure 1f) showed that the average discharge voltage was lowered by only 0.08 and 0.15 V at 2000 and 5000 mAh⁻¹, respectively. Briefly, the rate performance of Thn-CH₃COO in the 2 M Zn(CF₃SO₃)₂ electrolyte was among the highest level of OCMs for ARZBs. Moreover, we further examined its long-term cycling performance in this electrolyte (Figure 1g). Under a current rate of 1000 mAh⁻¹, the capacity of Thn-CH₃COO still remained 65% (relative to the reversible capacity of 158 mAh⁻¹ achieved at the 8th cycle) after 500 cycles, suggesting a good cycling stability (it seemed not as good as expected if comparing with that at 100 mAh⁻¹ in Figure 1b, which was probably caused by less uniform redeposition of the active material at higher current rate, leading to poorer contact with conductive carbon in the electrode and thus faster capacity fading, more clearly presented in Figure 1c).

Besides the galvanostatic discharge–charge method, we also conducted cyclic voltammetry (CV) and electrochemical impedance spectroscopy (EIS) tests of the Zn–Thn-CH₃COO cell with the 2 M Zn(CF₃SO₃)₂ electrolyte for further understanding of the electrochemical behaviors. The typical CV curves (Figure 2a) showed a pair of symmetric redox peaks at 0.7/0.9 V vs. Zn²⁺/Zn under a low scan rate of 0.1 mVs⁻¹, and considerable potential polarization with increase of scan rate (up to 2.0 mVs⁻¹). The relation between peak current (i_p) and scan rate (v) was analyzed by a linear fitting of $\lg(i_p)$ vs. $\lg(v)$ (Figure 2b), resulting in b values (in the equation of $i_p = a \times v^b$) of 0.65 and 0.58 in the cathodic and anodic processes, respectively. It suggested that the reaction kinetics of Thn-CH₃COO was controlled by hybrid solid diffusion and pseudocapacitive behaviors.^[22] Figure 2(c) shows the EIS data of the cell in charged state at different cycle numbers, which were fitted using a classic equivalent circuit (Table S2). The charge transfer resistance (R_{ct}) was 163 Ω at the pristine state, and significantly decreased to 73 Ω after the initial cycle, indicating that the Thn-CH₃COO electrode structure was optimized after a discharge-charge cycle, probably caused by its dissolution-redeposition behavior.^[23] Subsequently, the R_{ct} values gradually increased to 94, 288, and 925 Ω at the 5th, 20th, and 50th cycle, suggesting continuous deterioration of the electrode structure during repeated dissolution-redeposition processes.

To reveal the origin of capacity fading and the influence of electrolyte on it, we tested the solubility of Thn-CH₃COO in different electrolytes and discharge/charge states (Figure 3). The five electrolytes after immersing the pristine Thn-CH₃COO electrode showed different colors from light blue to dark purple (Figure 3a). The ultraviolet–visible (UV–Vis) spectra of them (Figure 3a) were in accordance with the visual observation and confirmed that the solubility was the lowest in 2 M Zn(CF₃SO₃)₂ electrolyte and the highest in 1 M Zn(CH₃COO)₂ and 3 M Zn(CF₃SO₃)₂ electrolytes. It strongly agreed with the tendency of cycling stability in these electrolytes, and verified that dissolution of Thn-CH₃COO was the key factor of capacity fading. It also suggested that CF₃SO₃⁻ had weaker interaction with Thn⁺ than CH₃COO⁻, but too concentrated CF₃SO₃⁻ anions would enhance the interaction of electrolyte and thus facilitate the dissolution of Thn-CH₃COO, which counteracted the

dissolution-Inhibition effect of decreased water activity and increased solution viscosity.^[24] Moreover, we examined the solubility of the Thn-CH₃COO electrode in different redox states (pristine, discharged to 0.2 V, and recharged to 1.6 V) in the same electrolyte of 2 M Zn(CF₃SO₃)₂, but no significant difference was observed.

In order to uncover the redox mechanism of Thn-CH₃COO, especially the kinds of cations and anions participating the bipolar reaction, a series of ex-situ characterization were conducted for the Thn-CH₃COO electrodes at different states (pristine, 0.2 V, and 1.6 V) of the discharge–charge process in the 2 M Zn(CF₃SO₃)₂ electrolyte (Figure 4). Firstly, the Fourier transform infrared (FTIR) spectra (Figure 4a) showed that after a whole cycle, the COO⁻ group (at 1605 and 1391 cm⁻¹) of CH₃COO⁻ anion^[25] still existed with high intensity, while the signals of SO₃⁻ group (at 1254 and 1027 cm⁻¹) of CF₃SO₃⁻ anion^[26] obviously appeared. It indicated that the extracted CH₃COO⁻ anions from Thn-CH₃COO in the discharge process largely restored into the active material in the subsequent charge process, with the co-insertion of CF₃SO₃⁻ anions from the electrolyte. It is worth noting that the mole number of CF₃SO₃⁻ anions in the electrolyte was two orders of magnitudes higher than that of CH₃COO⁻ from Thn-CH₃COO. Hence, the reason was probably that the extracted CH₃COO⁻ anions were still trapped in the electrode, and/or they had significantly stronger interaction with Thn⁺ than CF₃SO₃⁻, which was consistent with the tendency of solubilities (Figure 3a).

Figure 4(b) shows the X-ray diffraction (XRD) patterns of the three Thn-CH₃COO electrodes. After discharging to 0.2 V, there were many new diffraction peaks emerged, which almost completely disappeared after the subsequent charge process. They were attributed to the precipitated basic zinc trifluoromethanesulfonate [Zn_x(CF₃SO₃)_{2x-y}(OH)_y·nH₂O]^[12,27] and basic zinc acetate [Zn₅(CH₃COO)₂(OH)₈·2H₂O]^[28] as by-products of the consumption of H⁺. It also explained why the extracted CH₃COO⁻ anions was trapped in the electrode rather than diffused into the electrolyte, resulting in its reversible extraction/re-insertion. After recharging to 1.6 V, besides the characteristic peaks of Thn-CH₃COO, some other weak peaks were also observed, indicating the appearance of Thn-CF₃SO₃. In addition to the XRD method, we also performed the scanning electron microscopy (SEM) and energy dispersive spectroscopy (EDS) characterization of the surfaces of the electrodes (Figure 4c–h). Obviously, at 0.2 V a thin layer of flakes newly appeared and covered on the surface (Figure 4d), which completely disappeared at 1.6 V (Figure 4e). Besides, there was no significant difference of electrode morphology between the pristine and 1.6 V electrodes (Figure 4c, e), suggesting that the structure integrity of the electrode could be well maintained in spite of the dissolution. The EDS mapping exhibited that the flakes contained Zn, O, F, and S elements but no C element (Figures 4f–h and S2), further confirming that they were inorganic Zn_x(CF₃SO₃)_{2x-y}(OH)_y·nH₂O precipitate (the concentration of C was too low to be detected). In contrast, the bulk of the electrode contained C, N, F, and S elements but negligible Zn and O elements, suggesting that the embedded cation was dominantly H⁺ rather than Zn²⁺ and Zn(CF₃SO₃)⁺.

In addition, we employed density functional theory (DFT) calculations to explain the redox mechanism of Thn-CH₃COO. Firstly, the HOMO–LUMO energy levels of the naked molecules in different redox states (i.e., Thn⁺ cation, Thn[·] radical, and Thn[−] anion) were calculated and compared (Figures 5a and S3). For the first single-electron step between Thn⁺ and Thn[·], the redox potential is mainly determined by the LUMO energy of Thn⁺ (−3.44 eV, for accepting one electron). In contrast, for the second single-electron step between Thn[·] and Thn[−], the redox potential is approximately determined by the HOMO energy of Thn[−] (−3.56 eV, for denoting one electron). Due to the small gap between the two energies (0.12 eV), the whole two-electron reaction between Thn⁺ and Thn[−] possessed only a single plateau (Figure 1d–f).

Besides the HOMO–LUMO energy levels, we also calculated the geometrical configurations, molecular electrostatic potential (MESP) distribution, and Gibbs free energies of related molecules (Figures 5b and S3, Table S3). The optimized geometrical structures suggested that for Thn-CH₃COO and Thn-CF₃SO₃, CH₃COO[−] and CF₃SO₃[−] anions preferred to bond with the partially positive-charged NH₂ substituent of Thn⁺ cation, rather than the N or S atom in the phenothiazine unit. After accepting one electron and releasing the anion, the molecule was transformed to Thn[·] radical, in which the central N atom was intensively negative-charged. Hence, it tended to be the active site of the second step of reaction to associate with the embedded cation. Furthermore, we calculated the Gibbs free energy changes (ΔG) of the possible reduction reactions with different embedded ions. For the first step, there was no significant difference between the ΔG values of Thn-CH₃COO and Thn-CF₃SO₃ (−4.20 and −4.24 eV, respectively). It indicated that the binding energies of CH₃COO[−] and CF₃SO₃[−] anions with Thn⁺ cation were very close, and thereby the co-insertion was possible. For the second step, the ΔG of the reaction with H⁺ (−10.35 eV) was remarkably larger than that with Zn(CF₃SO₃)⁺ (−4.22 eV). The divalent Zn²⁺ cation was not taken into calculation because it needs two Thn[−] anions and the additional intermolecular interactions will make the comparison unreliable, however, the binding with Zn(CF₃SO₃)⁺ can be also regarded as the intermediate step of the binding with Zn²⁺. Therefore, H⁺ was more likely to be the dominant cation to coordinate with Thn[−], which agreed well with the above analysis on *ex-situ* characterization results.

In addition to the redox mechanism, the electrode structure evolution mechanism of Thn-CH₃COO was also investigated, by *ex-situ* FTIR, XRD, and SEM characterization conducted for the electrodes in charged state at different cycle numbers (pristine, 1, 2, 20, 50, and 100) (Figure 6). The FTIR spectra (Figure 6a) showed no obvious variation of the COO[−]/SO₃[−] peak intensity ratios during the whole cycling, suggesting that the co-insertion of CH₃COO[−] and CF₃SO₃[−] remained unchanged despite the numerical superiority of CF₃SO₃[−]. The XRD patterns (Figure 6b) also maintained identical after the initial cycle, indicating the excellent structure stability of the Thn-CH₃COO electrode. The SEM images (Figure 6c–h) displayed that the structure integrity of the electrode was well retained during the whole cycling, except that the surface became slightly loose at

the 50th and 100th cycle, which was caused by the dissolution of Thn-CH₃COO. These results indicated that although Thn-CH₃COO was inevitably soluble in the 2 M Zn(CF₃SO₃)₂ electrolyte, the redox reaction was highly reversible and the electrode structure kept integrated and stable during cycling, which were responsible for its high cycling stability (Figure 1b).

Conclusion

In summary, we investigated phenothiazine-based thionin (Thn-CH₃COO) as a novel bipolar-type OCM for ARZBs. As a commercially available material, it has a higher theoretical capacity of 186 mAh g^{−1} and probably higher structure stability than the reported analogue, MB. After the optimization of zinc salt and concentration of electrolyte, the 2 M Zn(CF₃SO₃)₂ electrolyte was chosen for further study. In this electrolyte, Thn-CH₃COO exhibited the lowest solubility and thus the best electrochemical performance, including a reversible capacity of 162 mAh g^{−1}, a flat discharge plateau at about 0.8 V vs. Zn²⁺/Zn, and excellent cycling stability (94% capacity retention after 100 cycles) and rate capability (70% capacity retention at 5000 mAh g^{−1} vs. 100 mAh g^{−1}). *Ex-situ* characterization and DFT calculations verified the two-electron bipolar redox mechanism of Thn-CH₃COO, and revealed the co-insertion of CH₃COO[−] and CF₃SO₃[−] for the p-type reaction and H⁺ insertion for the n-type reaction. The *ex-situ* characterization were also employed to monitor the structure evolution of the Thn-CH₃COO electrode, and proved its high redox reversibility and structure stability, in spite of the inevitably dissolution. This work not only provide a high-performance bipolar OCM for ARZBs, but also insightful mechanism understandings for the further development of this field.

Experimental Section

Coin-cell fabrication

Thionin (Thn-CH₃COO) was purchased from Acros Organics (with purity of 99.8%) and directly used to prepare the cathode. Firstly, 60 wt% Thn-CH₃COO powder, 30 wt% KB conductive carbon (Ketjenblack, EC-600JD), and 10 wt% polytetrafluoroethylene (PTFE, 10 wt% aqueous dispersion) binder were well mixed with the addition of isopropanol to form a homogeneous paste. The paste was rolled into a thin film, which was dried and punched into small disks (8 mm in diameter), and then pressed onto stainless steel meshes as current collectors. The mass loading of active material was controlled at 2–3 mg cm^{−2}. The KB electrodes were made up of 90 wt% KB and 10 wt% PTFE by the same method, with a mass loading of 1.0–1.5 mg cm^{−2}.

The aqueous electrolytes of 1 M ZnSO₄, 1 M Zn(CH₃COO)₂, and 1/2/3 M Zn(CF₃SO₃)₂ were simply prepared by dissolving a certain amount of zinc sulfate heptahydrate (ZnSO₄·7H₂O, 99%, Aladdin), zinc acetate [Zn(CH₃COO)₂, 99%, Adamas], and zinc trifluoromethanesulfonate [Zn(CF₃SO₃)₂, 99%, Bidepharm] into deionized (DI) water.

CR2016-type coin cells were assembled in ambient atmosphere by separating the zinc foil anode (12 mm in diameter and 0.2 mm in

thickness) and the Thn-CH₃COO (or KB) cathode with a glass fiber separator (Whatman, GF/A), which was soaked with approximately 100 μL of aqueous electrolyte.

Electrochemical tests

The as-prepared CR2016-type coin cells were employed for all electrochemical tests at room temperature. The galvanostatic discharge-charge tests were carried out on a battery test system (Neware, CT-4008T, China) in the voltage range of 0.2–1.6 V. The current rate was 100 mA g⁻¹ unless otherwise specified. The cyclic voltammetry (CV) and electrochemical impedance spectroscopy (EIS) measurements were performed on an electrochemical station (Princeton Applied Research, PRATAT MC, USA), in the same voltage range. For the CV tests, different scan rates of 0.1, 0.2, 0.5, 1.0, and 2.0 mV s⁻¹ were used for the same cell. For the EIS tests during cycling (100 mA g⁻¹), the data were recorded after charging to 1.6 V at different cycle numbers, with a frequency range of 10⁵–10⁻² Hz and a voltage amplitude of 10 mV.

Ex-situ characterization

For the dissolution tests, the Thn-CH₃COO electrodes (one-eighth rather than the whole piece was used to avoid making the solutions too concentrated for comparison) in different states (pristine, discharged to 0.2 V, and recharged to 1.6 V) were immersed in 2 mL of different electrolytes for 24 h. The phenomena were recorded by photography. In addition, the final solutions were characterized by ultraviolet-visible (UV-Vis) spectroscopy using the corresponding blank electrolyte as a reference, on a UV-Vis spectrophotometer (INESA, L8, China).

For other ex-situ characterization methods, the Thn-CH₃COO electrode films were pressed onto stainless steel sheets rather than meshes as current collectors. The free-standing Thn-CH₃COO electrode films in different states (pristine, discharged to 0.2 V, and charged to 1.6 V at different cycle numbers) were harvested for characterization. The cathode films were taken out by disassembling the cells in a nitrogen-filled glove box, and then washed several times with DI water to remove the residual electrolyte. For the X-ray diffraction (XRD) tests, the wet electrode films were directly characterized on an X-ray diffractometer (Rigaku, MiniFlex 600, Japan). For the Fourier transform infrared (FTIR) spectroscopy, the films were further dried at 80 °C under vacuum for 1 h to remove the free water. Then a tiny fraction of the film was dispersed in a KBr pellet, which was measured on a FTIR spectrometer (Bruker, ALPHA II, Germany). In addition, the scanning electron microscopy (SEM) and energy dispersive spectroscopy (EDS) observations of dried electrode films were conducted on a scanning electron microscopy (ZEISS, MERLIN Compact, Germany). All the sample preparation processes were implemented in a nitrogen-filled glovebox as much as possible to avoid exposure to air before characterization.

DFT calculations

All the density functional theory (DFT) calculations were performed using Gaussian 16 software.^[29] The B3LYP/6-31+G(d,p) level^[30] was chosen to compute the geometrical configurations, energy levels, molecular electrostatic potential (MESP) maps, electron configurations, and Gibbs free energies (*G*) of related molecules and ions. The solvation effect of electrolyte was considered by the SMD solvation model^[31] and water was selected as the solvent. The Gibbs free energy changes (ΔG) of the reduction reactions was

calculated by subtracting the total *G* of all reactants (excluding electrons) from that of all products.

Acknowledgements

We gratefully acknowledge financial support from the National Natural Science Foundation of China (Nos. 22179102 and 21975189), the National Key Research and Development Program of China (2022YFB2402201), and the Recruitment Program for Young Professionals. We also acknowledge the Core Research Facilities of CCMS (WHU) for access to SEM and EDS characterization, and Supercomputing Center of Wuhan University for supercomputing system.

Conflict of Interest

The authors declare no conflict of interest.

Data Availability Statement

The data that support the findings of this study are available in the supplementary material of this article.

Keywords: bipolar · organic electrode materials · phenothiazine · thionin · zinc batteries

- [1] a) Z. Tie, L. Liu, S. Deng, D. Zhao, Z. Niu, *Angew. Chem. Int. Ed.* **2020**, *59*, 4920–4924; *Angew. Chem.* **2020**, *132*, 4950–4954; b) G. Fang, J. Zhou, A. Pan, S. Liang, *ACS Energy Lett.* **2018**, *3*, 2480–2501.
- [2] a) J. Kim, Y. Kim, J. Yoo, G. Kwon, Y. Ko, K. Kang, *Nat. Rev. Mater.* **2023**, *8*, 54–70; b) J. Huang, Z. Guo, Y. Ma, D. Bin, Y. Wang, Y. Xia, *Small Methods* **2019**, *3*, 1800272.
- [3] P. Poizot, J. Gaubicher, S. Renault, L. Dubois, Y. Liang, Y. Yao, *Chem. Rev.* **2020**, *120*, 6490–6557.
- [4] Z. Song, H. Zhou, *Energy Environ. Sci.* **2013**, *6*, 2280–2301.
- [5] a) Z. Ye, S. Xie, Z. Cao, L. Wang, D. Xu, H. Zhang, J. Matz, P. Dong, H. Fang, J. Shen, M. Ye, *Energy Storage Mater.* **2021**, *37*, 378–386; b) Z. Song, L. Miao, H. Duan, L. Ruhmann, Y. Lv, D. Zhu, L. Li, L. Gan, M. Liu, *Angew. Chem. Int. Ed.* **2022**, *61*, e202208821.
- [6] Y. Gao, G. Li, F. Wang, J. Chu, P. Yu, B. Wang, H. Zhan, Z. Song, *Energy Storage Mater.* **2021**, *40*, 31–40.
- [7] Z. Lin, H.-Y. Shi, L. Lin, X. Yang, W. Wu, X. Sun, *Nat. Commun.* **2021**, *12*, 4424.
- [8] K. W. Nam, H. Kim, Y. Beldjoudi, T.-W. Kwon, D. J. Kim, J. F. Stoddart, *J. Am. Chem. Soc.* **2020**, *142*, 2541–2548.
- [9] Y. Wang, C. Wang, Z. Ni, Y. Gu, B. Wang, Z. Guo, Z. Wang, D. Bin, J. Ma, Y. Wang, *Adv. Mater.* **2020**, *32*, 2000338.
- [10] a) M. Na, Y. Oh, H. R. Byon, *Chem. Mater.* **2020**, *32*, 6990–6997; b) D. Chen, M. Lu, D. Cai, H. Yang, W. Han, *J. Energy Chem.* **2021**, *54*, 712–726.
- [11] G. Sun, B. Yang, X. Chen, Y. Wei, G. Yin, H. Zhang, Q. Liu, *Chem. Eng. J.* **2022**, *431*, 134253.
- [12] S. Zheng, D. Shi, D. Yan, Q. Wang, T. Sun, T. Ma, L. Li, D. He, Z. Tao, J. Chen, *Angew. Chem. Int. Ed.* **2022**, *61*, e202117511.
- [13] F. Wan, L. Zhang, X. Wang, S. Bi, Z. Niu, J. Chen, *Adv. Funct. Mater.* **2018**, *28*, 1804975.
- [14] L. Yan, Q. Zhu, Y. Qi, J. Xu, Y. Peng, J. Shu, J. Ma, Y. Wang, *Angew. Chem. Int. Ed.* **2022**, *61*, e202211107.
- [15] M. Tang, Q. Zhu, P. Hu, L. Jiang, R. Liu, J. Wang, L. Cheng, X. Zhang, W. Chen, H. Wang, *Adv. Funct. Mater.* **2021**, *31*, 2102011.

- [16] N. Wang, Z. Guo, Z. Ni, J. Xu, X. Qiu, J. Ma, P. Wei, Y. Wang, *Angew. Chem. Int. Ed.* **2021**, *60*, 20826–20832; *Angew. Chem.* **2021**, *133*, 20994–21000.
- [17] W. Yang, X. Du, J. Zhao, Z. Chen, J. Li, J. Xie, Y. Zhang, Z. Cui, Q. Kong, Z. Zhao, C. Wang, Q. Zhang, G. Cui, *Joule* **2020**, *4*, 1557–1574.
- [18] C.-Y. Chen, K. Matsumoto, K. Kubota, R. Hagiwara, Q. Xu, *Adv. Energy Mater.* **2019**, *9*, 1900196.
- [19] Y. Luo, F. Zheng, L. Liu, K. Lei, X. Hou, G. Xu, H. Meng, J. Shi, F. Li, *ChemSusChem* **2020**, *13*, 2239–2244.
- [20] T. Cai, Y. Han, Q. Lan, F. Wang, J. Chu, H. Zhan, Z. Song, *Energy Storage Mater.* **2020**, *31*, 318–327.
- [21] W. Wu, Z. Lin, H.-Y. Shi, L. Lin, X. Yang, Y. Song, X.-X. Liu, X. Sun, *Chem. Eng. J.* **2022**, *427*, 131988.
- [22] Z. Chen, J. Wang, T. Cai, Z. Hu, J. Chu, F. Wang, X. Gan, Z. Song, *ACS Appl. Mater. Interfaces* **2022**, *14*, 27994–28003.
- [23] M. Li, Q. Wang, J. Wang, L. Huang, J. Chu, X. Gan, Z. Song, *Chem. Eng. J.* **2023**, *456*, 141114.
- [24] Q. Zhang, Z. Yang, H. Ji, X. Zeng, Y. Tang, D. Sun, H. Wang, *SusMat* **2021**, *1*, 432–447.
- [25] J.-L. Chen, L.-Y. Zhang, Z.-N. Chen, L.-B. Gao, M. Abe, Y. Sasaki, *Inorg. Chem.* **2004**, *43*, 1481–1490.
- [26] a) S. Chen, K. Li, K. S. Hui, J. Zhang, *Adv. Funct. Mater.* **2020**, *30*, 2003890; b) N. Munir, S. Masood, F. Liaqat, M. N. Tahir, S. Yousuf, S. Kalsoom, E. U. Mughal, S. H. Sumrra, A. Maalik, M. N. Zafar, *RSC Adv.* **2019**, *9*, 37986–38000.
- [27] Y. Dai, J. Li, L. Chen, K. Le, Z. Cai, Q. An, L. Zhang, L. Mai, *ACS Energy Lett.* **2021**, *6*, 684–686.
- [28] E. Hosono, S. Fujihara, T. Kimura, H. Imai, *J. Colloid Interface Sci.* **2004**, *272*, 391–398.
- [29] M. J. Frisch, G. W. Trucks, H. B. Schlegel, G. E. Scuseria, M. A. Robb, J. R. Cheeseman, G. Scalmani, V. Barone, G. A. Petersson, H. Nakatsuji, X. Li, M. Caricato, A. V. Marenich, J. Bloino, B. G. Janesko, R. Gomperts, B. Mennucci, H. P. Hratchian, J. V. Ortiz, A. F. Izmaylov, J. L. Sonnenberg, Williams, F. Ding, F. Lipparini, F. Egidi, J. Goings, B. Peng, A. Petrone, T. Henderson, D. Ranasinghe, V. G. Zakrzewski, J. Gao, N. Rega, G. Zheng, W. Liang, M. Hada, M. Ehara, K. Toyota, R. Fukuda, J. Hasegawa, M. Ishida, T. Nakajima, Y. Honda, O. Kitao, H. Nakai, T. Vreven, K. Throssell, J. A. Montgomery Jr., J. E. Peralta, F. Ogliaro, M. J. Bearpark, J. J. Heyd, E. N. Brothers, K. N. Kudin, V. N. Staroverov, T. A. Keith, R. Kobayashi, J. Normand, K. RagHAVACHARI, A. P. Rendell, J. C. Burant, S. S. Iyengar, J. Tomasi, M. Cossi, J. M. Millam, M. Klene, C. Adamo, R. Cammi, J. W. Ochterski, R. L. Martin, K. Morokuma, O. Farkas, J. B. Foresman, D. J. Fox, Wallingford, CT 2016.
- [30] K. C. Kim, T. Liu, S. W. Lee, S. S. Jang, *J. Am. Chem. Soc.* **2016**, *138*, 2374–2382.
- [31] A. V. Marenich, C. J. Cramer, D. G. Truhlar, *J. Phys. Chem. B* **2009**, *113*, 6378–6396.

Manuscript received: January 10, 2023

Revised manuscript received: January 22, 2023

Accepted manuscript online: January 24, 2023

Version of record online: February 6, 2023